Check for updates

Power Balance Partition Control Based on Topology Characteristics of Multi-Source Energy Storage Nodes

Songqing Cheng[1], Yun Teng[1]*, Hao Zuo[1] and Zhe Chen[2]

[1]The Department of Electrical Engineering, Shenyang University of Technology, Shenyang, China, [2]The Department of Energy Technology, Aalborg University, Aalborg, Denmark

Aiming at the power balance control of multi-source energy storage grid in the case of a high proportion of new energy grid connection. In this article, a power grid dynamic partition method based on the Markov energy field principle and a priori knowledge model is proposed. Combined with the coordinated dispatching of power grid source-load, a two-layer power balance partition control model based on the topological characteristics of multi-source energy storage nodes is established. First, in the upper-layer model, the energy homogenization method of multi-source energy storage nodes is studied, and the Markov energy field model of power grid node partition based on energy interaction constraints between nodes is established to partition the power grid initially. Combined with the prior model of node dynamic partition, the initial partition is dynamically optimized to realize the dynamic partition of the multi-source energy storage grid. Then, in the lower-layer model, the source-load coordinated dispatching model in the power grid partition area is established to realize the dynamic partition control of the power grid. Finally, based on the real operation data of a northeast power grid and IEEE39 node system, a dynamic partition power control simulation model of a multi-source energy storage power grid is established. The simulation results and analysis show that the dynamic partition power control strategy proposed in this article can effectively improve the regulation ability and economy of the power grid.

Keywords: multi-energy storage, energy correlation, Markov random field, source-load coordinated dispatching, power balance dynamic partition control

1 INTRODUCTION

With the proposal and steady implementation of the energy Internet strategy all over the world, the access scale and proportion of various energy forms of load and energy storage equipment, single machine high-capacity, and distributed renewable energy power generation equipment in the power system are also growing rapidly.

On the one hand, the growth of multiple energy forms and renewable energy access scale can not only effectively promote the upgrading of the energy industry and the improvement of sustainable energy utilization levels but also provide more and more effective dynamic and transient power control methods for power system (Sun et al., 2021). On the other hand, the complex topology and energy conversion relationship between load and energy storage among various energy forms (Chao etal., 2022; Qingfeng etal., 2022), as well as the randomness of renewable energy fluctuations, will bring new challenges to the power balance ability and emergency power control of power system
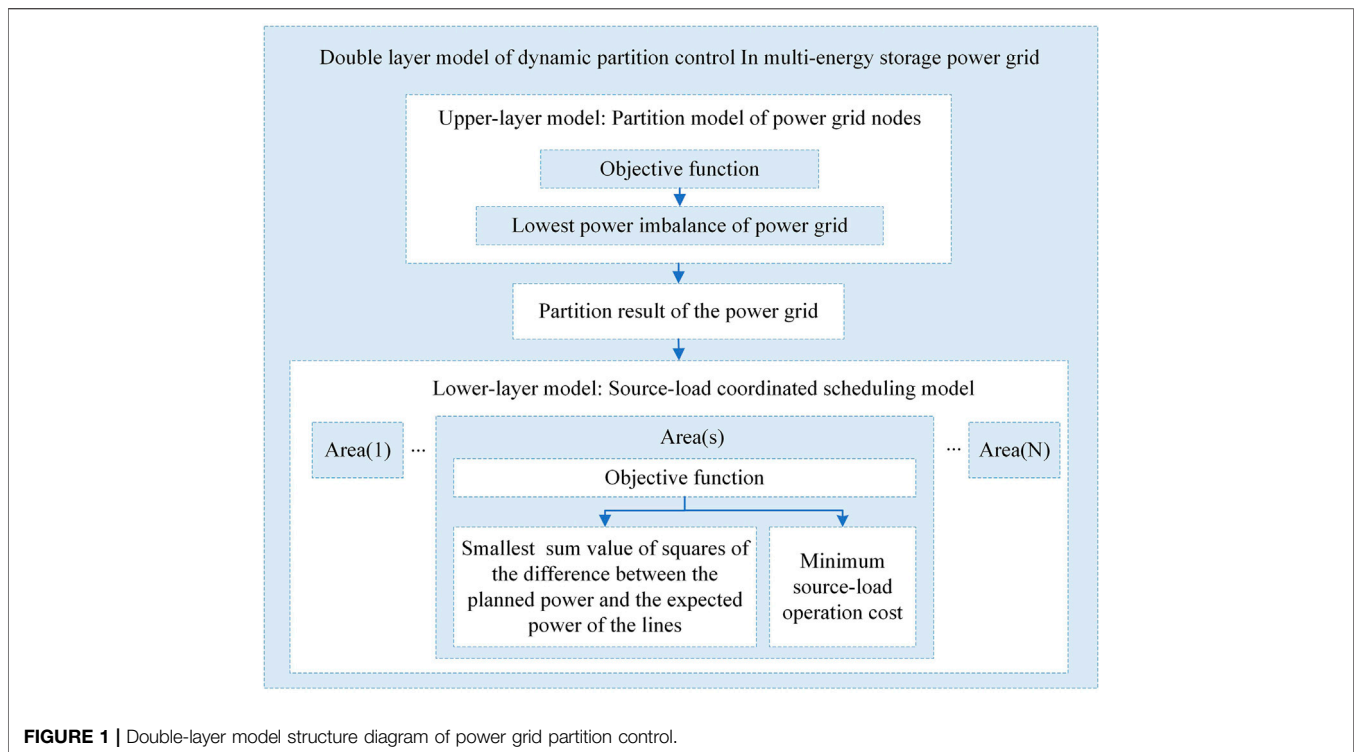
FIGURE 1 | Double-layer model structure diagram of power grid partition control.

(Yun et al., 2019), (Yun et al., 2018; Teng et al., 2019). Therefore, in the process of dynamic optimal control of the new energy grid, how to carry out distributed coordinated control of the system according to the multi-source energy storage support capacity and the fluctuation characteristics of renewable energy has attracted extensive attention of scholars on a global scale (Zhuang et al., 2022; Lili et al., 2022). It is also one of the hotspots and difficulties in the field of energy Internet at present.

Scholars have done a lot of research on the stability control of the power grid after a high proportion of new energy is connected to the grid. Feng et al. (2017) proposed a homogenized energy function model, which can realize the combined control of thermoelectricity after a new energy grid connection. Ruifeng et al. (2019), Rui et al. (2022) proposed the control mode of applying a cloud platform in a power system. Yun et al. (2019) proposed an electrothermal hydrogen multi-energy storage system to reduce wind and light abandonment. Li et al. (2021) established a community-integrated energy system with an electric vehicle charging station, which improved the regulation flexibility and economy of the power grid.

When the traditional method is used for power balance control, the object to be optimized is generally determined according to the operation experience and remains unchanged for a long time. This regulation method is often difficult to adapt to the complex and changeable power grid operation mode, and the optimization effect of the whole network is poor. With the expansion of the scale of high proportion new energy power grids, there are more and more uncertain factors, and the limitations of existing methods are gradually exposed. The establishment of a

power grid zoning control model is an effective way of power balance control.

In terms of power grid zoning operation control, Leng et al. (2021) proposed a multi provincial power grid power balance zoning control method under the condition of high renewable energy penetration. By predicting and correcting the transmission loss of each province under the future operation mode, the power of the tie line is consistent with the dispatching plan. Wu et al. (2021) proposed a grid parallel recovery zoning method which is helpful to speed up the black start recovery. Chai et al.(2018) proposed a double-layer voltage control strategy based on distribution network zoning to control the output of photovoltaic units to minimize power grid loss.

Based on the existing research results aiming at the power balance control problem of multi-source energy storage networks under the condition of a high proportion of new energy grid connections, a two-layer model of power balance zoning control based on the topological characteristics of multi-source energy storage nodes is established in this article. In the upper-layer model, the prior model of node dynamic zoning is studied, and the initial zoning is dynamically optimized to realize the dynamic zoning of the multi-source energy storage grid. In the lower-layer model, the source load coordinated dispatching model in the power grid zoning area is established to realize the dynamic zoning control of the power grid. In addition, based on the real operation data of a northeast power grid and IEEE39 node system, a dynamic partition power control simulation model of a multi-source energy storage power grid is established. The simulation results and analysis show that the dynamic partition

power control strategy proposed in this article can effectively improve the regulation ability and economy of the power grid.

2 PARTITION CONTROL MODEL STRUCTURE OF POWER BALANCE IN POWER GRID WITH MULTI-ENERGY STORAGE SYSTEM

In order to realize the power balance partition control under the condition of a large-scale new energy grid connection, a double-layer model (Kuo et al., 2022) of power balance partition control based on a multi-source energy storage grid is established in this article. The structure diagram of the double-layer control model is shown in **Figure 1**.

In the upper-layer model, this article analyzes the energy homogenization of multi-source energy storage nodes and comprehensively grasps the energy interaction of the power grid through the established power grid dynamic partition energy prior model. Taking the minimum energy imbalance of the power grid as the objective function, the power grid partition problem is transformed into the minimization of energy imbalance, and the preliminary power grid partition scheme is formed.

In the lower-layer model, taking the minimum difference between the expected power and the actual power and the minimum operation cost as the double objective function, the optimal source load coordinated scheduling scheme is obtained under the source load operation constraint.

After the upper-layer and lower-layer models are solved, the lower-layer objective function value is returned to the upper-layer. After repeated iterative correction, the grid partition control scheme with the optimal characteristics is finally obtained.

3 PARTITION MODEL OF MULTI-SOURCE ENERGY STORAGE POWER GRID

3.1 Energy Homogenization Model of Multi-Source Energy Storage Nodes

Due to the large difference and low compatibility of multiple heterogeneous energy models in multi-source energy storage, it is necessary to clarify the coupling mechanism and basic law of multiple energy sources. Before establishing the node energy topology model, based on the factor analysis method, a heterogeneous energy homogenization characterization model is established to uniformly characterize the output power of heterogeneous energy (Ye et al., 2020).

Based on the idea of factor analysis, a variety of power series are modeled. The output power of the power supply at each time is regarded as a multidimensional original variable. Suppose that the standardized d day hourly output power sequence of a power supply at time i is $P_i = [p_{i,1} \cdots p_{i,j} \cdots p_{i,d}]$. Then the

standardized power sequence p of the power supply can be represented by the hourly output power sequence of the corresponding t longitudinal times, which can be expressed as **Eq. 1**.

$$\mathbf{P} = \begin{bmatrix} p_{1,1} & \cdots & p_{1,j} & \cdots & p_{1,d} \\ \vdots & \ddots & \vdots & \ddots & \vdots \\ p_{i,1} & \cdots & p_{i,j} & \cdots & p_{i,d} \\ \vdots & \ddots & \vdots & \ddots & \vdots \\ p_{t,1} & \cdots & p_{t,j} & \cdots & p_{t,d} \end{bmatrix}, \qquad (1)$$

where t is the sampling points of the power supply in day d, and $p_{i,j}$ is the standardized power of the power supply by day j time i. Factor analysis is carried out on the standardized sample matrix $\mathbf{P}$, and ρ is the homogenization scale parameters of multi-energy hybrid nodes. The common factor matrix is $\mathbf{F} = [F_1 \cdots F_j \cdots F_m]^T$. The special factor matrix is $\boldsymbol{\varepsilon} = [\varepsilon_1 \cdots \varepsilon_j \cdots \varepsilon_m]^T$. Then, the factor analysis model of the power supply composed of the sum of common component ρF and special component is as follows:

$$\mathbf{P} = \rho \mathbf{F} + \boldsymbol{\varepsilon}, \qquad (2)$$

In **Eq. 2**, we can see that the homogenization scale parameters ρ explains the correlation between power $\mathbf{P}$ and common factor $\mathbf{F}$. The common component $\rho \mathbf{F}$ explains the common information of the power curve of the power supply. The special component $\boldsymbol{\varepsilon}$ represents the part of the power series at each time that cannot be explained by the common factor, which is an unobservable hidden variable.

3.2 Correlation Degree Model of Multi-Source Energy Storage Nodes

When partitioning the power grid, set the power grid represented by the node set as follows:

$$X = \{x_1, x_2, ..., x_s\}, \qquad (3)$$

where $x_s, x_r \in X$ are any two adjacent nodes in grid X, and S is the total number of nodes in grid X.

Let node x_u be a node that has energy interaction with both x_s and x_r. The more energy interaction among x_u, x_s, and x_r, the greater the correlation between x_s and x_r. Conversely, the less energy interaction among x_u, x_s, and x_r, the fewer the correlation between x_s and x_r.

The topological energy correlation degree t_{sr} of two adjacent nodes x_s, x_r is defined as follows:

$$t_{sr} = \begin{cases} \dfrac{a_{sr} + \sum\limits_{u \neq s,r} a_{su} a_{ru}}{\min\left\{\sum\limits_{u \neq s} a_{su}, \sum\limits_{u \neq r} a_{ru}\right\} + 1 - a_{sr}}, & s \neq r \\ 1, & s = r \end{cases}, \qquad (4)$$

where $a_{sr} = dist(x_s, x_r)$ indicates the degree of energy homogenization of x_s and x_r $(0 \leq a_{sr} \leq 1)$, and $\sum\limits_{u \neq s,r} a_{su} a_{ru}$ is the energy storage sharing degree between x_s and x_r.

It can be seen from **Eq. 2** that the greater the number of nodes x_u and energy interaction with two adjacent nodes x_s and x_r in the power grid, the greater the topological energy correlation degree of the two nodes is, and vice versa. Then the node topology energy incidence matrix of the power grid can be obtained as follows:

$$T(X) = [t_{sr}]_{s,r \leq S}. \tag{5}$$

In the power grid, only two nodes with branch connection can have energy interaction. Therefore, the grid node topology incidence matrix of **Eq. 5** is a symmetric and non-negative matrix.

3.3 Partition Model of Multi-Source Energy Storage Network

It is assumed that a local area of the power grid represented by equivalent power grid nodes is as follows:

$$O = \{O_s | s \in S\}, \tag{6}$$

where $S = \{s | s \leq M \times N\}$ represents a finite node set in the power grid, and the capacity of the node set is $M \times N$, O_s is the adjacent node set of node S with energy interaction.

If a grid area is known as follows:

$$X = \{x_s | x_s \in \Omega, s \in S\}, \tag{7}$$

where $\Omega = [-1, 1]$ is the energy storage demand of node x_s in the power grid, which indicates at the node with multi-source energy storage device access, the requiring variation range of the operating state of the energy storage device may be from 100% rated power charging to 100% rated power discharging.

Let the injected energy of node x_s be y_s, and divide the power grid into several regions. Then the energy field of the power grid in each region can be obtained, which could be expressed as follows:

$$Y = \{y_s | y_s \in \Lambda, s \in S\}, \tag{8}$$

where $\Lambda = \{0, 1, ..., L\}$ is the aggregate of power grid partition area. The grid partition energy field divided in **Eq. 8** is regarded as a Markov random field (Zhao et al., 2020). Then the probability of obtaining the partitioned energy field Y in the given power grid X is as follows:

$$P(Y|X) = \frac{P(X|Y)P(Y)}{P(X)}, \tag{9}$$

In the switching process of the power grid operation state, the dynamic solution process of the power grid partition energy field Y is transformed into the process of obtaining its global optimal estimation solution Y^*. The estimation problem of the global optimal partition energy field Y^* can be transformed into the minimization problem of power grid energy imbalance. The transformation process can be expressed as:
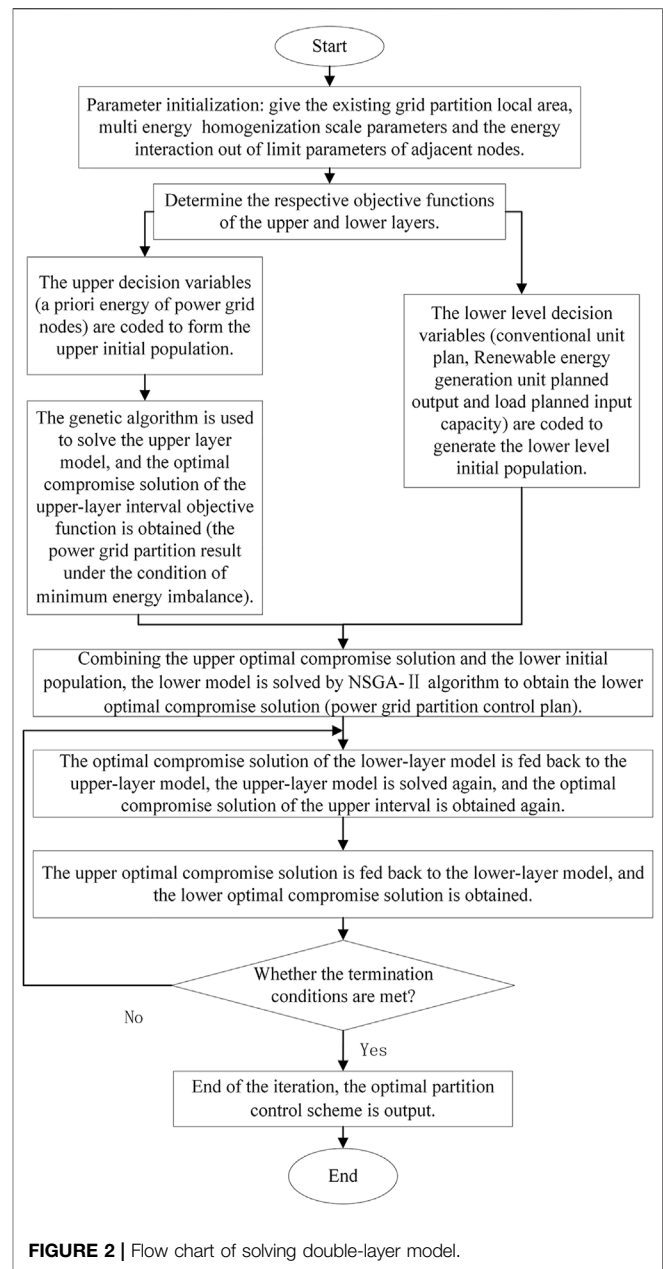
FIGURE 2 | Flow chart of solving double-layer model.

$$\begin{aligned} Y^* &= \arg \max_Y P(Y|X) \\ &\sim \arg \min_Y E_g(X,Y) \\ &= \arg \min_Y \{E_d(X,Y) + E_s(Y)\} \end{aligned} \tag{10}$$

where $E_g(X,Y)$ is the energy imbalance of grid X under energy field Y, $E_d(X,Y) = -\lg P(X|Y)$ is the energy shortage in partition area, $E_s(Y) = \sum_{s,r \in N(s)} \delta(y_s, y_r)$ is the available energy of multi-source energy storage in the partition area, and $N(s)$ is the neighborhood node of grid node S.

3.4 A Priori Model for Dynamic Partition of Multi-Source Energy Storage Grid

In the dynamic partition process of multi-source energy storage power grid, the global energy balance information of power grid is the key prior knowledge for the dynamic adjustment of the power grid partition aiming at energy balance. In addition, the global energy information is described by the correlation degree between power grid nodes, especially multi-source energy storage nodes.

However, the energy correlation degree between simple nodes couldn't fully reflect the spatial characteristics of the power grid energy field. Therefore, it is necessary to establish a prior model of dynamic partition of a multi-source energy storage grid (Lai and Chiang, 2008) to describe the global energy of the grid and dynamically optimize the grid partition algorithm.

Let w_s be the number of nodes in a local area with direct or cascade energy interaction with node y_s in the power grid. Then the total number of nodes in the local area is $|w_s| \times |w_s|$.

Let $y_r \in O_s(y_s)$ represent a subset of the regional node set of node y_s, and $O_s(y_s)$ is an aggregate of adjacent nodes with direct energy interaction in the region w_s of node y_s. Then, the energy correlation degree $t_{sr}(x_s, x_r)$ of any two adjacent nodes x_s and x_r is as follows:

$$t_{sr}(x_s, x_r) = \begin{cases} \dfrac{a_{sr} + \sum\limits_{u \neq s,r} a_{su} a_{ru}}{\min\left\{ \sum\limits_{u \neq s} a_{su}, \sum\limits_{u \neq r} a_{ru} \right\} + 1 - a_{sr}}, & s \neq r \\ 1, & s = r \end{cases} \tag{11}$$

where a_{sr} is the energy interaction intensity between nodes x_s and x_r.

$$a_{sr} = \left| \exp\left\{ \frac{-2 \times (\|x_s - x_r\|_2)^2}{\left(\rho \max\limits_{r \in N_s} \|x_s - x_r\|_2 \right)^2} \right\} \right|^{\gamma}, \tag{12}$$

where $\|x_s - x_r\|_2$ is the Euclidean distance between adjacent contacts, ρ is the homogenization scale parameters of multi energy hybrid nodes, and $\gamma(\gamma \geq 1)$ is the energy interaction out of limit penalty factor between adjacent nodes.

It can be seen from **Eq. 11** and **12** that if nodes x_s and x_r each have high energy correlation with multiple shared nodes, and nodes x_s and x_r are a pair of adjacent nodes, then, according to the nature of energy transfer, this pair of adjacent nodes have a high degree of energy correlation, and vice versa.

According to the established energy correlation degree model of power grid nodes, it can be seen that the prior of high-order topological space of node correlation degree $t_{w_s}(x_s, x_{O_s})$ in local area w_s of power grid is as follows:

$$t_{w_s}(x_s, x_{o_s}) = t_{N1}(x_s, x_{N1}) + t_{N2}(x_s, x_{N2}) + \cdots + t_{Ni}(x_s, x_{Ni}), \tag{13}$$

where $t_{N1}(\cdot), t_{N2}(\cdot), \ldots, t_{Ni}(\cdot)$, respectively, represent the topological energy correlation degree of node x_s and all of its adjacent nodes with energy interaction in the local regional topology of the power grid.

That is, the value of the prior high-order topological space of node correlation degree $t_{w_s}(x_s, x_{O_s})$ is the sum of the energy correlation degrees $t_{Ni}(\cdot)$ of node x_s and its adjacent nodes in the region.

Therefore, based on the node correlation degree model and the energy correlation degree high-order topological space prior model, a high-order priori energy model can be established to describe the topological correlation degree of power grid nodes as follows:

$$E_h(x_w|B) = \sum_{N \in S, r \in N_s} \left[\frac{a_{sr} + \sum\limits_{u \neq s,r} a_{su} a_{ru}}{\min\left\{ \sum\limits_{u \neq s} a_{su} \sum\limits_{u \neq r} a_{ru} \right\} + 1 - a_{sr}} \right], \tag{14}$$

where $E_h(x_w|B)$ is the high-order priori energy, and $B = \{\rho, \gamma\}$ is the parameters of high-order prior model for power grid partition.

To sum up, this article establishes a prior model of power grid dynamic partition. First, based on the existing partition topology, the energy correlation degree model between power grid nodes is established. Then, on this basis, a priori model of high-order topological space is established to describe the strength of energy correlation of all nodes in the region. Finally, a high-order energy prior model is established to control the overall energy interaction in the power grid partition.

4 COORDINATED DISPATCHING MODEL OF SOURCE-LOAD IN POWER GRID PARTITION AREA

4.1 Objective Function

The lower-layer model takes the minimization of the square sum of the difference between the planned power and the expected power in the scheduling cycle and the minimization of the source load operation cost as the double objectives (Gu and Chen, 2021; Mengzeng et al., 2022; Xiaojie et al., 2022; Jiang et al., 2022). That is, on the premise of considering the economy, find the power grid partition area endogenous load coordinated dispatching plan to maximize the expected power. The object functions could be expressed as follows:

$$\min F_1 = \sum_{l \in L_{pa}} \sum_{t=1}^{T} \left(P_{l,t}^{\text{plan}} - P_{l,t}^{\text{exp}} \right)^2, \tag{15}$$

$$\min F_2 = \sum_{s=1}^{N} \left(C_s^G + C_s^W + C_s^P + C_s^L \right), \tag{16}$$

where $P_{l,t}^{plan}$ is the planned power of line l in t period, $P_{l,t}^{\exp}$ is the expected power of line l in t period, L_{pa} is the aggregate of the grid partition line, N is the number of grid partition areas, $C_s^G, C_s^W, C_s^P, C_s^L$, respectively, represent the generation cost of conventional unit, abandonment cost of wind power and photovoltaic power, and load regulation cost.

The calculation formulas of various costs are as follows:
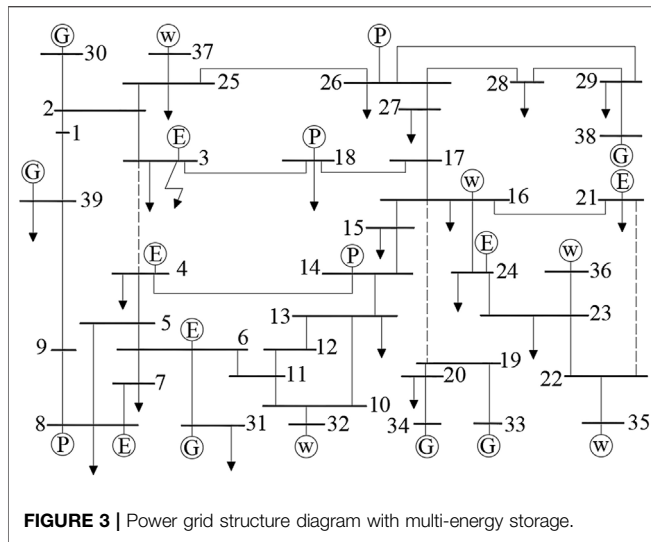
FIGURE 3 | Power grid structure diagram with multi-energy storage.

$$C_s^G = \sum_{t=1}^{T} \sum_{i=1}^{G_s} \alpha_i P_{i,t}^G \Delta t, \tag{17}$$

$$C_s^W = \sum_{t=1}^{T} \sum_{j=1}^{W_s} \sigma_j \left(P_{j,t}^{W,\,\mathrm{fore}} - P_{j,t}^{W} \right) \Delta t, \tag{18}$$

$$C_s^P = \sum_{t=1}^{T} \sum_{k=1}^{P_s} \lambda_k \left(P_{k,t}^{\mathrm{Ph,fore}} - P_{k,t}^{\mathrm{Ph}} \right) \Delta t, \tag{19}$$

$$C_s^L = \sum_{t=1}^{T} \sum_{l=1}^{L_s} \mu_h P_{l,t}^L \Delta t, \tag{20}$$

where $P_{i,t}^G$ is the planned output of conventional unit i during the time period of t, α_i is the unit generation cost of conventional unit i, $P_{j,t}^W$, $P_{k,t}^{Ph}$, respectively, represent the planned output of wind power field j and photoelectric station k during the time period of t, $P_{j,t}^{W,\,fore}$, $P_{k,t}^{Ph,fore}$, respectively, represent the day ahead forecast output of wind power field j and photoelectric station k during the time period of t, σ_j, λ_k respectively represent the cost of wind power and photovoltaic power abandonment per unit capacity of wind power field j and photoelectric station k, $P_{l,t}^L$ is the planned input capacity of load during the time period of t, G_S, W_S, P_S, H_S, respectively, represent the number of conventional unit, wind power field, photovoltaic power station and load.

The calculation formula of planned power $P_{l,t}^{plan}$ is as follows:

$$\sum_{l \in L_i} P_{l,t}^{plan} = \sum_{i=1}^{G_s} P_{i,t}^G + \sum_{j=1}^{W_s} P_{j,t}^W + \sum_{k=1}^{P_s} P_{k,t}^{Ph} - \sum_{l=1}^{L_s} P_{l,t}^L - P_{Load,t}^s, \tag{21}$$

where $P_{Load,t}^s$ represents the general load forecast value for the time period of t in partition area of s, and L_i is the aggregate of lines contained in the transmission line of partition area s.

4.2 Constraint Condition
4.2.1 Output Constraints of Renewable Energy

$$0 \leq P_{RE}^t \leq P_{RE}^f, \tag{22}$$

where P_{RE}^f is the forecast value of renewable energy output, and P_{RE}^t is the real value of renewable energy output.

4.2.2 Output Constraints of Thermal Power Units

$$P_i^{\min} \leq P_i^t \leq P_i^{\max}, \tag{23}$$

where $P_i^{\max}$, $P_i^{\min}$, and P_i^t, respectively, represent the upper and lower limits of output and the actual output value of thermal power unit i.

4.2.3 Climbing Constraint of Thermal Power Unit

$$\begin{cases} \sum_{i=1}^{G} \left(P_i^t - P_i^{t-1} \right) \leq R_{\mathrm{up}} \\ \sum_{i=1}^{G} \left(P_i^{t-1} - P_i^t \right) \leq R_{\mathrm{down}} \end{cases}, \tag{24}$$

where R_{up} and R_{down}, respectively, represent upward and downward climbing rate of thermal power unit.

4.2.4 Constraint of Power Balance

$$\sum_{i=1}^{G} P_i^t + \sum_{j=1}^{W} P_j^{RE} = P_L, \tag{25}$$

where P_L is the total load of the power grid partition area.

4.2.5 Constraint of Multi-Source Energy Storage
4.2.5.1 Constraint of Electrothermal Hybrid Energy Storage
Considering the complexity of electrothermal hybrid energy storage operation, in order to better control the virtual energy storage equipment, a power state function is introduced. It can be expressed as follows:

$$\begin{cases} dP_{ETSS,E,in} / dt = a_1, P_{ETSS,E,in\,min} \leq P_{ETSS,E,in} \leq P_{ETSS,E,\,in\,max} \\ dP_{ETSS,T,in} / dt = a_2, P_{ETSS,T,in\,min} \leq P_{ETSS,T,in} \leq P_{ETSS,T,in\,max} \\ dP_{ETSS,E,out} / dt = a_3, P_{ETSS,E,out\,min} \leq P_{ETSS,E,out} \leq P_{ETSS,E,out\,max} \\ dP_{ETSS,T,out} / dt = a_4, P_{ETSS,T,out\,min} \leq P_{ETSS,T,out} \leq P_{ETSS,T,out\,max} \end{cases}, \tag{26}$$

Where $P_{ETSS,E,in\,\min}$, $P_{ETSS,E,out\,\min}$, $P_{ETSS,T,in\,\min}$, and $P_{ETSS,T,out\,\min}$, respectively, represent the minimum value of the input electric power, output electric power, input thermal power, and output thermal power of the electrothermal hybrid energy storage. $P_{ETSS,E,\,in\,\max}$, $P_{ETSS,T,in\,\max}$, $P_{ETSS,E,out\,\max}$, and $P_{ETSS,T,out\,\max}$, respectively, represent the maximum value of the input electric power, output electric power, input thermal power, and output thermal power of the electrothermal hybrid energy storage. a_1 is the state function of electrothermal hybrid energy storage power. It can simulate the charge and discharge rate of battery energy storage, and there is $a_{l\,\min} \leq a_l \leq a_{l\,\max}$, $l = 1, 2, 3, 4$.

TABLE 1 | Parameters of the power grid with multi-energy storage.

DC transmission/MW	Thermal power installed capacity/MW	Wind power installed capacity/MW	Photovoltaic power installed capacity/MW	Electricity storage capacity/MWh	Heat storage capacity /MWh	Hydrogen storage capacity/MWh
300	6000	3000	1200	300	400	300

4.2.5.2 Power Constraint of Electric Hydrogen Production Equipment

$$\begin{cases} 0 \le P_{EH}(t) \le P_{EH,\max} \\ \Delta P_{EH,\min} \le \Delta P_{EH}(t) \le \Delta P_{EH,\max} \end{cases}, \quad (27)$$

where $P_{EH}(t)$ is the power consumption of electric hydrogen production equipment during the time period of t, $P_{EH,\max}$ is the maximum power consumption of electric hydrogen production equipment, $\Delta P_{EH}(t)$ is the variation of input power of electric hydrogen production equipment during the time period of t, $\Delta P_{EH,\max}$ and $\Delta P_{EH,\min}$, respectively, represent the maximum and minimum climbing rate of electric hydrogen production equipment.

4.2.5.3 Constraints of Hydrogen and Heat Storage Equipment

In order to ensure the stable operation of energy storage equipment, the following constraints shall be met:

$$\begin{cases} W_{S,\min} \le W(t) \le W_{S,\max} \\ P_{S,\min} \le P_S(t) \le P_{S,\max} \\ S_{OH,\min} \le S_{OH}(t) \le S_{OH,\max} \\ S_{OT,\min} \le S_{OT}(t) \le S_{OT,\max} \end{cases}, \quad (28)$$

Where $W(t)$ is the energy storage capacity of hydrogen and heat storage equipment during the time period of t, $W_{S,\max}$ and $W_{S,\min}$, respectively, represent the upper and lower limits of energy storage equipment, $P_S(t)$ is the output power of energy storage equipment during the time period of t, $P_{S,\max}$ and $P_{S,\min}$, respectively, represent the maximum value of charging and discharging energy of energy storage equipment, $S_{OH}(t)$ is the residual hydrogen of energy storage equipment during the time period of t, $S_{OH,\max}$ and $S_{OH,\min}$, respectively, represent the upper and lower limits of residual hydrogen of hydrogen storage equipment, $S_{OT}(t)$ is the residual heat of heat storage equipment, $S_{OT,\min}$ and $S_{OT,\max}$, respectively, represent the minimum and maximum values of residual heat state of heat storage equipment.

4.2.6 Load Constraint

According to the characteristics of load participating in demand side response, the load can be divided into conventional load and adjustable load. In addition, the adjustable load can be divided into translatable load and interruptible load.

4.2.6.1 Constraint of Conventional Load Fluctuation

$$V_{cl,t} \le V_{cl,\max}, \quad (29)$$

where $V_{cl,t}$ is the fluctuation rate of conventional load, and $V_{cl,\max}$ is the maximum fluctuation rate of conventional load.

4.2.6.2 Constraint of Adjustable Load

Constraint of interruptible load can be expressed as follows:

$$\begin{cases} P_k^{\min} \le P_{k,t} \le P_k^{\max} \quad k \in n_f \\ 0 \le M_j \le n_{T,j}^{\max} \quad j \in n_T \\ V_{IL,i}^{total} \le V_{IL,i}^{\max} \end{cases}, \quad (30)$$

where $P_{k,t}$, $P_k^{\max}$ and $P_k^{\min}$, respectively, represent the actual power and upper and lower limits of power of interruptible load, M_j is the actual number of calls of interruptible load, $n_{T,j}^{\max}$ is the maximum number of calls of interruptible load, $V_{IL,i}^{total}$ is the total interruption time in scheduling cycle, and $V_{IL,i}^{\max}$ is the maximum reduction time in scheduling cycle.

Constraint of translatable load can be expressed as follows:

$$\begin{cases} P_{y,j}(t) - P_{y,j}(t-1) \le P_{y,j}^{\max} \\ \sum_{t=1}^{T} P_{y,j}(t) \times \Delta t = \sum_{t=1}^{T} P_{y0,j}(t) \times \Delta t \end{cases}, \quad (31)$$

where $P_{y,j}(t)$ is the power of translatable load after response of the time period of t, $P_{y,j}^{\max}$ is the maximum allowable variation power of translatable load, and $P_{y0,j}(t)$ is the original power of translatable load during the time period of t.

5 MODEL SOLVING

When solving, the upper-layer model selects the genetic algorithm suitable for a single objective solution. In the preliminary zoning, it is necessary to conduct a comprehensive and rapid search for the power supply area. Therefore, the GA algorithm with both rapid random search ability and simultaneous comparison of multiple individuals is selected for a solution, and the process of the genetic algorithm is relatively simple, which can make the solution process easier. NSGA-II algorithm suitable for a double-objective solution is selected in the lower model, and the index of 'congestion distance' is introduced to select individuals, which has a simple structure and good convergence. The upper-layer and lower-layer transfer the optimal compromise solution to each other and iteratively solve the double-layer model until the termination conditions are met. The specific solution process is shown in **Figure 2**.

The upper-layer and lower-layer models will each solve a set of optimal solution sets. Therefore, this paper uses the fuzzy membership function method to construct the membership function separately for the optimization goal, changes it to the

FIGURE 4 | Variation curves of power supply in the power grid without energy storage device.

FIGURE 6 | Grid power adjustment curve with multi-energy storage.

FIGURE 5 | Variation curves of load power in the power grid without energy storage device.

FIGURE 7 | The distribution space of the optimal solution of the upper-layer model.
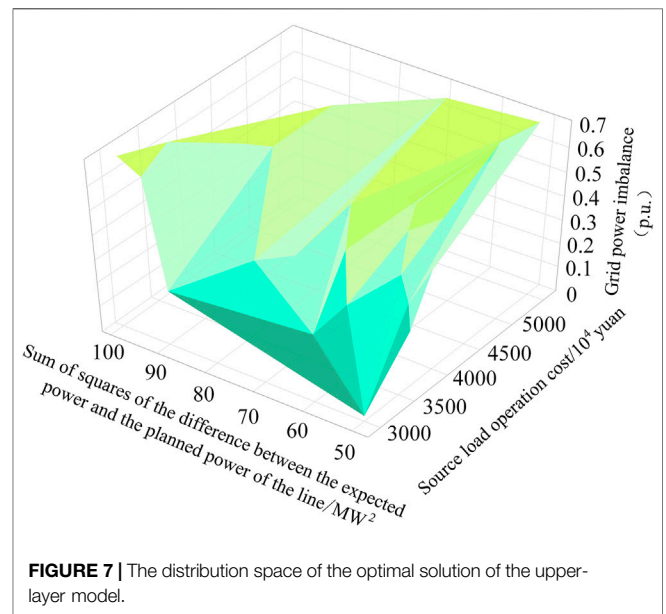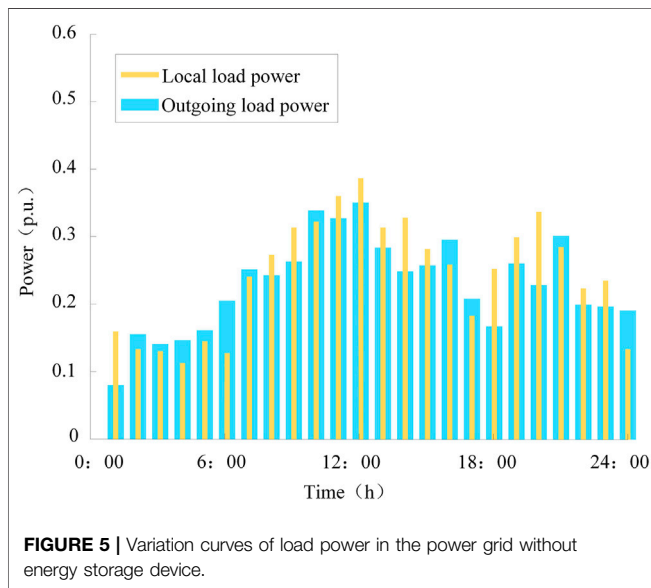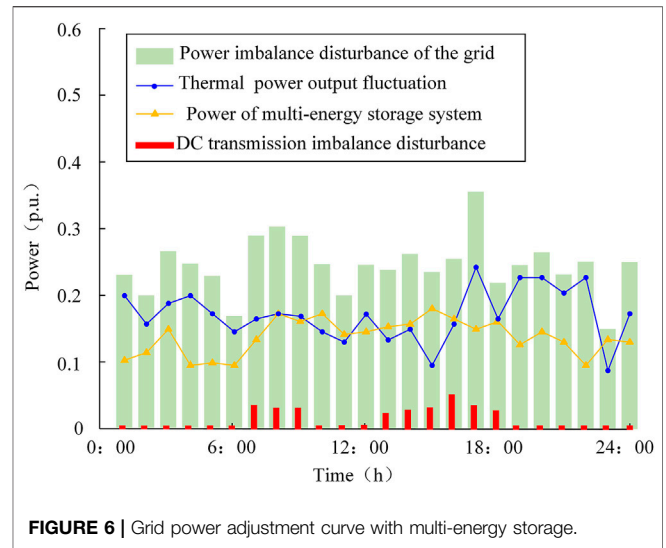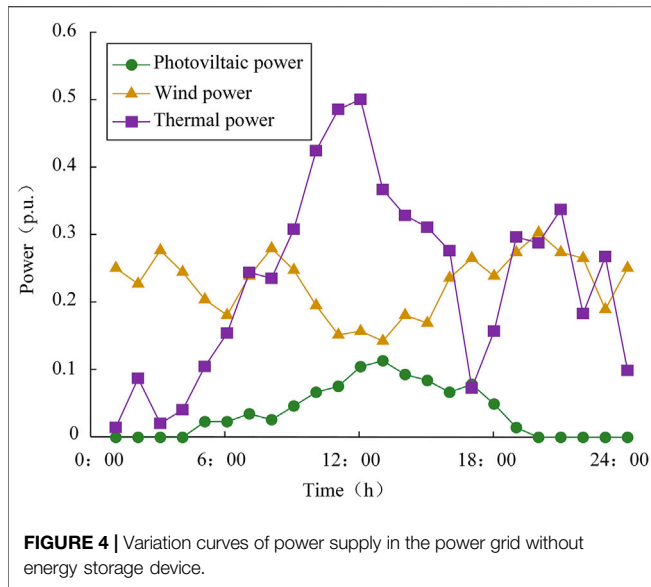
degree of compliance with the optimization results, and finds the optimal compromise solution through the comparison of the degree of compliance with the optimization goal.

6 SIMULATION ANALYSIS

Based on the multi-source operation data of a multi-source energy storage grid in northeast China, combined with the IEEE39 node system, the simulation verification is carried out. The established simulation model of the multi-source energy storage grid is shown in **Figure 3**.

As can be seen from **Figure 3**, there are six thermal power supply (GE) nodes, five wind power supply (WP) nodes, four photovoltaic power supply (PV) nodes, and six multi-energy

storage (ES) nodes in the system. The solid line in the system diagram is the AC line and the dotted line is the DC line.

The grid load in **Figure 3** includes local load and outgoing load. The parameters of system power supply, energy storage, and DC transmission capacity are shown in **Table 1**.

When the multi-energy storage device does not work in the power grid, the typical daily variation curves of wind power, photovoltaic, thermal power, local load and outgoing load in the power grid are shown in **Figures 4** and **5**.

It can be seen from **Figures 4** and **5** that due to the fluctuation characteristics of renewable energy output in the power grid, when the total load demand of the power grid changes, in order to meet the power balance requirements, the output of thermal power units must be adjusted according to the total power imbalance. Therefore, when the proportion of renewable

FIGURE 8 | The distribution plane of the optimal solution of the lower-layer model.

FIGURE 10 | Different algorithms for the best values.

FIGURE 9 | Grid power adjustment curve of the power grid with proposed dynamic partition control.
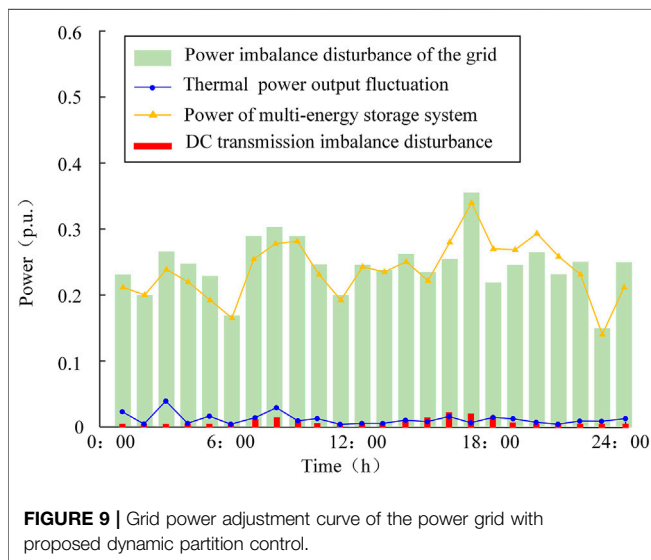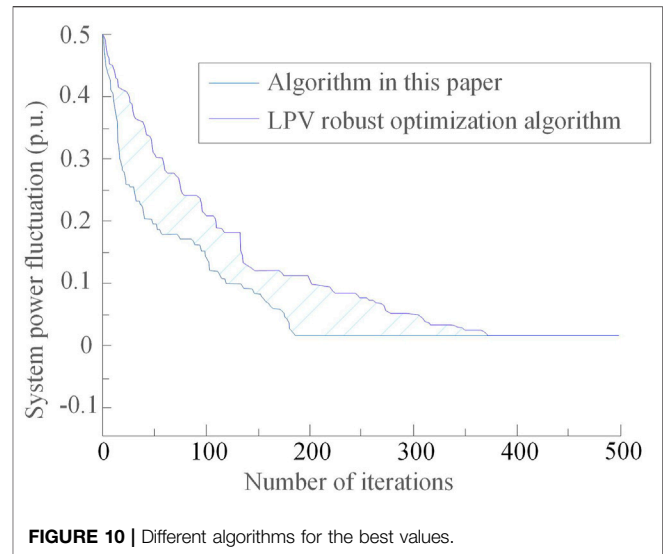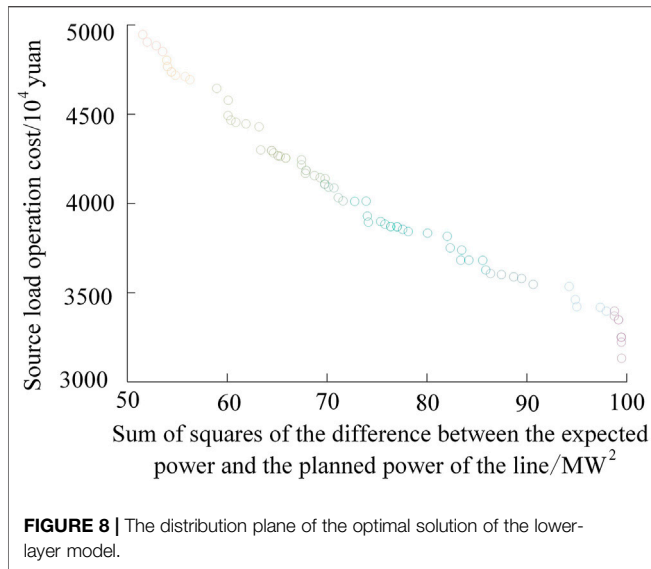
energy is high, it will cause greater peak shaving pressure on thermal power units.

After multi-source energy storage is configured, the power imbalance disturbance of the grid, thermal power output fluctuation, total charge and discharge power of multi-source energy storage system, and DC transmission imbalance disturbance daily change curves are shown in **Figure 6**.

It can be seen from **Figure 6** that after multiple nodes in the power grid are configured with multi-source energy storage, the total power imbalance of the power grid can be borne by multi-source energy storage. However, as the output of the thermal power unit and energy storage system is required to shave the peak for the load, the transmission power of the connected DC line may change. Therefore, the greater the peak valley difference of power grid load and the inverse peak regulation characteristics of renewable energy output, the greater the possibility of DC line power change.

The power grid dynamic partition control algorithm proposed in this article is used to simulate the partition optimal control of the power imbalance disturbance of the system in **Figure 3**. The control parameters are multi-energy homogenization scale parameter $\rho = 0.33$, energy out of limit penalty factor $\gamma = 1.16$, the number of iterations of the model is 300, the algebra of genetic algorithm is 1500, and the population size is 200. Tournament selection operator and two-point crossover operator are adopted. The crossover probability is 0.9 and the reorganization probability is 0.6.

Solve the upper-layer and lower-layer models, and finally get two groups of optimal solutions with a wide distribution range. **Figure 7** shows the distribution of the optimal solution of the upper-layer model in the objective function space.

Figure 8 shows the distribution of the optimal compromise solution of the upper-layer model corresponding to the optimal solution of the lower-layer model on the objective function plane.

According to the method proposed in this article, the dynamic partition control of the power grid is carried out. At this time, the power imbalance disturbance of the grid, thermal power output fluctuation, total charge and discharge power of multi-source energy storage system, and DC transmission imbalance disturbance daily change curves are shown in **Figure 9**.

As can be seen from **Figure 9**, under the disturbance of the same unbalanced power of the power grid, the power grid dynamic partition control strategy proposed in this article can analyze the high-order priori energy of new energy nodes and multi-source energy storage nodes in the power grid, so as to realize the partition coordination of power imbalance.

The simulation results show that using by multi-source energy storage to absorb renewable energy power, the output time and regulation capacity of thermal power units in the power grid are significantly reduced, the power change of DC transmission line is vastly reduced, and the regulation capacity of the power grid is improved. The effectiveness of the power grid dynamic partition power control method proposed in this paper is verified.

In order to highlight the advantages of this algorithm, it is compared with LPV robust optimization in reference (Li et al., 2018). The convergence curve of the optimal solution is shown in **Figure 10**. It can be seen that the convergence speed of the power grid dynamic zoning method proposed in this article is much faster than that of the LPV robust optimization method, which further proves the superiority of the method proposed in this article. At the same time, although the convergence of the algorithm is optimistic at present, the complexity of the algorithm is slightly higher. Therefore, the research should continue with the goal of simplifying the algorithm in the future.

7 SUMMARY

Aiming at the control problem of power imbalance under the fluctuation of the new energy output of power grid with multi-source energy storage, this article studies the double-layer model of power grid dynamic partition power control considering the topology of multi-source energy storage nodes. First, the multi-source energy storage nodes are described homogeneously, and the prior energy model of power grid topology is established to

provide the basis for power grid partition. Then, considering the operation characteristics of source and load, the source and load coordinated dispatching model is established to realize the dynamic partition power control of the power grid. Finally, based on the actual data, the established model is simulated and solved. The results show that the obtained power grid dynamic partition control plan is effective and can provide scientific decision-making basis for dispatchers.

DATA AVAILABILITY STATEMENT

The original contributions presented in the study are included in the article/Supplementary Material, further inquiries can be directed to the corresponding author.

AUTHOR CONTRIBUTIONS

SC was responsible for the specific work of this manuscript. YT and ZC guided the work of this manuscript. HZ carried out some of the calculation work.

REFERENCES

Chai, Y., Guo, L., Wang, C., Zhao, Z., Du, X., and Pan, J. (2018). Network Partition and Voltage Coordination Control for Distribution Networks with High Penetration of Distributed PV Units. *IEEE Trans. Power Syst.* 33 (3), 3396–3407. doi:10.1109/TPWRS.2018.2813400

Chao, W., Hao, H., Lian, Z., Tiezhou, W., Min, Z., and Tiao, B. (2022). Photovoltaic Energy Storage System Based on Smart Battery and its Control Strategy[J]. *Renewable Energy Resources* 40 (4), 506–512. doi:10.13941/j.cnki.21-1469/tk.2022.04.018

Feng, L., Hao, Y., Tieyan, Z., Yun, T., and Qian, H. (2017). "Research on Homogenization Modeling and Planning Method of Thermoelectric Combined System," in 2017 10th International Conference on Intelligent Computation Technology and Automation (ICICTA), Changsha, China, 9-10 Oct. 2017, 217–220. doi:10.1109/ICICTA.2017.55

Gu, X., and Chen, Z. (2021). "Multi-time-scale Scheduling Optimization of Regional Multi-Energy Systems Considering Source-Load Uncertainty," in 2021 13th International Conference on Measuring Technology and Mechatronics Automation (ICMTMA), Beihai, China, 16-17 Jan. 2021, 198–201. doi:10.1109/ICMTMA52658.2021.00051

Guili, Y., Zhenmin, W., Huaqi, L., Jianfang, Y., and Fang, F. (2022). Short-Term Wind Power Prediction Based on Deep Belief Network[J]. *Acta Energiae Solaris Sinica* 43 (2), 451–457. doi:10.19912/j.0254-0096.tynxb.2020-0405

Kuo, S., Xuefei, Z., Fujian, C., Guixin, L., Tao, L., and Liang, Z. (2022). Optimal Configuration and Control Strategy of Hybrid Energy Storage System for Smoothing Wind Power Fluctuations[J]. *Renewable Energy Resources* 40 (3), 402–409. doi:10.13941/j.cnki.21-1469/tk.2022.03.015

Jiang, W., Jingjing, W., Qiang, Z., and Yachao, Z. (2022). Two-Stage Robust Cooperative Scheduling for Electricity-Gas Integrated Energy System Considering Power-To-Pas or Wind Power Accommodation[J]. *Acta Energiae Solaris Sinica* 43 (2), 436–443. doi:10.19912/j.0254-0096.tynxb.2020-0340

Lai, K. R., and Chiang, Y.-Y. (2008). "A Constraint-Based Framework for Incorporating A Priori Knowledge into Fuzzy Modelling," in 2008 IEEE International Conference on Fuzzy Systems (IEEE World Congress on Computational Intelligence), Hong Kong, China, 1-6 June 2008, 1811–1817. doi:10.1109/FUZZY.2008.4630616

Leng, Y., Yang, C., Chang, L., Zhang, Y., and Wang, Z. (2021). "Partition Control Method of Power Balance of Multi.Provincial Grid with High Penetration of

Renewable Energy," in The 10th Renewable Power Generation Conference (RPG 2021), Online Conference, 14-15 Oct. 2021, 168–173. doi:10.1049/icp.2021.2246

Li, Y., Han, M., Yang, Z., and Li, G. (2021). Coordinating Flexible Demand Response and Renewable Uncertainties for Scheduling of Community Integrated Energy Systems with an Electric Vehicle Charging Station: A Bi-level Approach. *IEEE Trans. Sustain. Energ.* 12 (4), 2321–2331. doi:10.1109/TSTE.2021.3090463

Li, Y., Teng, Y., Leng, O., and Yuan, S. (2018). Transient Stability Linear Parameter Varying Robust Feedback Control for Interconnected Power System by Wind Power AC/DC Channel. *[J]. Renew. Energ. Resour.* 36 (4), 557–562. doi:10.13941/j.cnki.21-1469/tk.2018.04.014

Lili, Z., Yue, X., Xiaohe, Y., Chiyu, L., and Jing, G. (2022). Risk and Benefit Evaluation for Energy Storage Under Differentiated Markets[J]. *Acta Energiae Solaris Sinica* 43 (3), 111–118. doi:10.19912/j.0254-0096.tynxb.2020-0504

Mengzeng, C., Yixin, H., Shuo, Y., Liang, C., and Jinqi, L. (2022). A Multi-Sourceload Complementary Integration Planning Method Based on Energy Behavior Analysis[J]. *Renewable Energy Resources* 40 (4), 527–535. doi:10.13941/j.cnki.21-1469/tk.2022.04.011

Qingfeng, W., Zeying, Z., Shaojuan, Y., and Zhicheng, Z. (2022). Soh Balancing Scheme for Distributed Energy Storage Systems in Microgrid Based on Multi-Agent[J]. *Acta Energiae Solaris Sinica* 43 (2), 104–112. doi:10.19912/j.0254-0096.tynxb.2020-0404

Rui, L., Kuihua, W., Liang, F., Rong, L., Xian, W., and Shenquan, Y. (2022). Voltage Partition Coordinated Optimization Control of Active Distribution Network of High Penetration Distributed Pvs[J]. *Acta Energiae Solaris Sinica* 43 (2), 189–197. doi:10.19912/j.0254-0096.tynxb.2020-0239

Ruifeng, Z., Shiming, L., Yang, L., Bin, W., Wenxin, G., and Jiangang, L. (2019). "Application Analysis and Prospect of Cloud Platform in Operation Control of New Energy Power System," in 2019 IEEE 9th Annual International Conference on CYBER Technology in Automation, Control, and Intelligent Systems (CYBER), Suzhou, China, 29 July-2 Aug. 2019, 980–985. doi:10.1109/CYBER46603.2019.9066672

Sun, Y., Teng, Y., and Yang, S. (2021). "Optimization Model of Multi-Energy System Based on Multi-Source Energy Storage," in 2021 13th International Conference on Measuring Technology and Mechatronics Automation (ICMTMA), 16-17 Jan. 2021Beihai, China, 216–219. doi:10.1109/ICMTMA52658.2021.00055

Teng, Y., Sun, P., Hui, Q., Li, Y., and Chen, Z. (2019). A Model of Electro-thermal Hybrid Energy Storage System for Autonomous Control Capability

Enhancement of Multi-Energy Microgrid. *Csee Jpes* 5 (4), 489–497. doi:10.17775/CSEEJPES.2019.00220

Wu, Y., Li, Q., Li, Q., Chen, D., Yu, X., and Lin, J. (2021). "Optimal Partition for Power System Restoration," in 2021 IEEE 4th International Electrical and Energy Conference (CIEEC), Wuhan, China, 28-30 May 2021, 1–6. doi:10.1109/CIEEC50170.2021.9510697

Xiaojie, P., Wenchao, Z., Youping, X., Junwei, Y., Meng, Z., and Dejun, S. (2022). The stability risk optimization for power system considering multi-source load uncertainty[J]. *Renewable Energy Resources* 40 (3), 396–401. doi:10.13941/j.cnki.21-1469/tk.2022.03.013

Ye, L., Qu, X., Ma, M., Yao, Y., and Wang, W. (2020). Multi-energy System Homogeneous Coupling Model Considering Wind-Photovoltaic-Hydro Power Generations[J]. *Power Syst. Technol.* 44 (09), 3201–3210. doi:10.13335/j.1000-3673.pst.2020.0771

Yun, T., Zedi, W., Yan, L., Qian, M., Qian, H., and Shubin, L. (2019). A Multi Energy Storage System Model Based on Electricity Heat and Hydrogen Coordinated Optimization for Power Grid Flexibility. *Csee Jpes* 5 (2), 266–274. doi:10.17775/CSEEJPES.2019.00190

Yun, T., Tieyan, Z., and Zhe, C. (2018). Review of Operation Optimization and Control of Multi-Energy Interconnection System Based on Micro-Grid[J]. *Renewable Energy Resources* 36 (3), 467–474. doi:10.13941/j.cnki.21-1469/tk.2018.03.022

Zhao, J., Li, L., Xu, Z., Wang, X., Wang, H., and Shao, X. (2020). Full-Scale Distribution System Topology Identification Using Markov Random Field. *IEEE Trans. Smart Grid* 11 (6), 4714–4726. doi:10.1109/TSG.2020.2995164

Zhuang, Z., Hongli, Z., and Cong, W. (2022). Research on Optimization of "Sourcenet-Charge-Storage" Operation of Regional Energy Internet[J]. *Renewable Energy Resources* 40 (2), 238–246. doi:10.13941/j.cnki.21-1469/tk.2022.02.012